Advanced Composite Materials
Publication details, including instructions for authors and subscription information:
http://www.tandfonline.com/loi/tacm20

Processing and characterization of carbon-carbon nanofiber composites

Rahul Jain , Uday K. Vaidya & Anwarul Haque

Version of record first published: 02 Apr 2012.

To cite this article: Rahul Jain , Uday K. Vaidya & Anwarul Haque (2006): Processing and characterization of carbon-carbon nanofiber composites, Advanced Composite Materials, 15:2, 211-241

To link to this article: http://dx.doi.org/10.1163/156855106777873905

Adv. Composite Mater., Vol. 15, No. 2, pp. 211–241 (2006)

Also available online - www.vsppub.com

Processing and characterization of carbon-carbon nanofiber composites *

RAHUL JAIN [1], UDAY K. VAIDYA [1,†] and ANWARUL HAQUE [2]

[1] *Department of Materials Science and Engineering, 1530 3rd Avenue South, BEC-254, The University of Alabama at Birmingham, Birmingham, Alabama 35294-4461, USA*
[2] *Department of Aerospace & Engineering Mechanics, The University of Alabama, Tuscaloosa, Alabama 35487-0280, USA*

Received 29 October 2005; accepted 16 November 2005

Abstract—Carbon-carbon composites (CCCs) have extremely high thermal stability and shock resistance and find use in aerospace applications and aircraft disk brakes. The processing of CCCs can be divided into three stages: curing of precursor resin/fiber-reinforced-laminate; carbonization; and densification. During carbonization, the precursor resin (such as phenolic and furfuryl alcohol) develops microcracks and oftentimes delaminations, which reduce the mechanical properties of the material. In this study, we investigated the influence of carbon nanofibers (CNFs) when mixed with phenolic matrix precursor on the microstructure and interlaminar shear strength (ILSS) of the as-cured and carbonized composite specimens. CNFs offer low cost benefits, unlike traditional carbon nanotubes (CNTs) that tend to be expensive. Different loadings (0%, 2%, and 5% weight/weight of resin) of CNFs, in conjunction with various percentages of surfactant (0%, 12.5%, and 50% by weight of acetone) treated carbon fabric reinforcement were used for the study. The rationale for treating the fabric with surfactant was to vary interfacial conditions of reinforcing fiber-CNF-matrix. This paper outlines the work done in the processing of CCC-CNF composites, and the influence of surfactant and various percentages of CNFs on the resulting microstructure and ILSS properties. The use of CNFs provided a bridging mechanism for matrix microcracking and reducing matrix shrinkage that occurs during first carbonization. Porosity and delaminations were found to increase with increase in surfactant treatment. An inverse relationship was observed between ILSS and porosity. At the as-cured and carbonized stages, an optimal value of 2% CNFs yielded the highest ILSS values of ∼40 MPa and 6 MPa respectively.

Keywords: Carbon nanofibers (CNFs); carbon-carbon composite (CCC); carbonization; microcracking.

*Edited by the JSCM.

†To whom correspondence should be addressed. E-mail: uvaidya@uab.edu

1. INTRODUCTION

Carbon-carbon composites (CCCs) are increasingly being used because of their strength retention at high temperatures (> 2500°C) and high resistance to thermal shocks. CCCs find applications in sporting goods, automobiles, biomedical implants, aircraft brakes, and nozzle cones for atmospheric reentry vehicles [1–3]. The application of a CCC in any field requires tight process control. The processing defines the microstructure, mechanical, thermal, and electrical characteristics of the final material. Carbon fiber (C-fiber) reinforced phenolic composites can be converted to CCCs through carbonization (heating in an inert atmosphere of gaseous nitrogen) and subsequent densification cycles. The typical manufacturing steps for a CCC are shown in Fig. 1. During the carbonization of the composite, various volatiles are generated and the structure is converted to carbon. Due to the differences in thermal contraction existing between the resin matrix and the C-fiber reinforcement, they undergo different degrees of contraction. These two phenomena (volatile emanation and contraction) lead to porosity and micro-crack generation in the composite, and in some cases, debonding/delamination of the individual layers. Gao *et al.* [4] discussed the various types of voids and cracks that can occur during the carbonization of a CCC and their dependency on the fiber weave type.

Many researchers have investigated the effects of addition of graphite powder, pitch, and other micro-particles on the resulting structure and properties of CCCs. Kang and Jeong [5] modified phenolic resin by adding micro-size particles of pitch and graphite. They reported decrease in mechanical property of the green

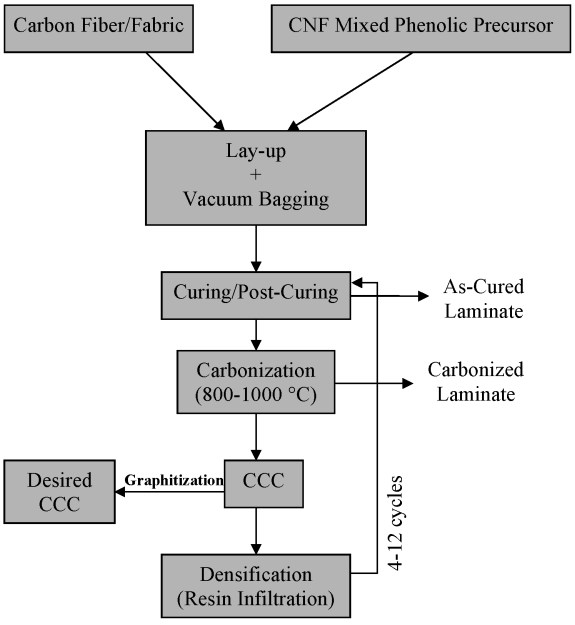

Figure 1. Schematic of the CNFs modified CCCs processing.

composite (as cured) with increase in powder content. However, higher mechanical property of the CCC was observed for the powder modified matrix precursors. Ma *et al.* [6] studied the effect of inorganic silica on the microstructure, physical, and morphological properties of CCCs. They found that voids caused by the degradation of phenolic resin were filled by small particles composed of elemental C, Si, and O, consequently decreasing the porosity. Furthermore, they reported improved interfacial bonding of the ceramer-derived carbon matrix and fibers as compared to phenolic-resin derived carbon matrix and fibers. Yasuda *et al.* [7] studied the effect of graphite powder addition on the microstructure of carbon matrix in CCCs as well as neat carbon. They reported that the addition of graphite powder retarded the polymerization of the resin and reduced shrinkage during carbonization. When graphite powder mixed resin was used for making C-fiber composite, the shrinkage reduced during the carbonization. The flexural strength was observed to increase up to small loadings of graphite powder (5%), after which the strength was found to decrease. They attributed this to the ductility provided by the graphite fibers to the matrix, which resulted in fiber pull-out during testing instead of brittle fracture. Hung *et al.* [8] modified the novolac-type phenolic resin with polyethylene-oxide (PEO). They reported a decrease in density of PEO/phenolic resin blend-derived CCC with increase in PEO content. Lin *et al.* [9] reported an improved oxidation resistance of CCC derived from phenolic resin/silica hybrid ceramers. Müller *et al.* [10] discussed the effect of coating the C-fiber with polysiloxane and phenolic resin on the mechanical properties. They found that the coating reduced the adhesion between C-fiber and phenolic matrix, which translated into improved flexural strength and modulus. Zaldivar *et al.* [11] used boron in the form of a carborane ($C_2B_{10}H_{12}$) compound to catalytically graphitize a polyarylacetylene resin in the CCC. They reported that the tensile strength was improved due to fiber pull-out and suggested that interface weakening occurred which decreased the tendency for matrix-dominated brittle fracture. Ma *et al.* [12] discussed that good chemical bonding between the C-fiber and the matrix before the carbonization can result in higher ILSS, but poor flexural properties after carbonization. Tai *et al.* [13] reinforced phenolic matrix with multi-walled nanotubes (MWNTs) and reported an improvement in Young's modulus and yield stress. They showed the CNT-pullout from the matrix in the fractured specimen through SEM studies. From their studies, it can be inferred that weakening of the interface facilitates toughening mechanisms such as crack bridging and fiber pullout. Tzeng and Chr [14], after measuring the weight loss, open porosity and microstructure observation, reported an increase in porosity in CCC below 600°C due to decomposition of phenolic resin matrix, and crack development above 600°C. Since the phenolic resin above 600°C was converted to glassy carbon, the corresponding CCC showed matrix-dominated brittle fracture behavior with low fiber strength utilization.

The premise of the present work is that a nanostructured matrix could be used to control the microstructure evolution of CCCs. In this work, we have used CNFs because of their cost-effectiveness in comparison to CNTs. A recent survey by

the Air Force Research Laboratory (AFRL) projected CNFs to be commercially available at $3 per pound over the next decade [15]. As compared to CNTs, handling and microanalysis of CNFs is easier. CNFs have diameters in the range of 60–150 nm, inner diameters or hollow cores of 30–90 nm, and their length varies from 30–100 μm. This geometry gives them aspect ratios of 200–1667. Baker [16] showed that CNFs consist of graphite platelets perfectly arranged in various orientations with respect to the fiber axis, giving rise to varied conformations. Patton *et al.* [17] used CNFs to reinforce the epoxy matrix and observed an increase in stiffness and flexural strength. They acknowledged that the voids, residual thermal strains (because of very high surface area of CNFs), fiber–matrix bonding, and the degree of dispersion, could cause loss in strength. Sandler *et al.* [18] used standard polymer processing technique such as extrusion and injection molding to produce CNF reinforced poly(ether-ether-ketone) composite. They found an increase in tensile stiffness and strength with CNF loading fractions up to 15 wt%. Lozano *et al.* [19] conducted rheological and microscopic analysis and showed that the high shear processing of polypropylene/CNF mixture led to homogenous dispersion of CNFs without agglomeration or curtailment. Tibbetts *et al.* [20] produced CNF/nylon and CNF/polypropylene composite and reported an increase in tensile strength and modulus after loading the polymers with CNFs.

CNTs and CNFs tend to agglomerate in the matrix because of their electrical and magnetic properties. Various types of surfactants have hence been investigated by different researchers to study dispersion of CNTs in polymers. Santos *et al.* [21] used non-ionic surfactant Triton X-100, Vigolo *et al.* [22] used anionic surfactant sodium dodecyl sulfate, Bandow *et al.* [23] used cationic surfactant benzalkonium chloride, Gong *et al.* [24] and Ranta and Bakis [25] used non-ionic surfactant polyoxyethylene-8-lauryl ether for studies dealing with dispersion of CNTs in polymers. Similar surfactants can be used for the effective dispersion of CNFs in the resin. For the application of CNTs or CNFs in CCCs, it hence becomes imperative to consider the effect of surfactant in CCCs. It is of interest to determine how the surfactant changes the interfacial characteristics of the fiber and matrix; density, porosity, micro-cracks, and carbon yield after the first carbonization; and its effects on the mechanical properties of the composite.

Although CCCs modified with materials other than CNFs have been explored by various researchers, the use of CNFs in CCCs is relatively new. The idea is to use CNF-mixed phenolic matrix precursor for impregnating the reinforcing fibers to achieve controlled porosity and microcracks. The controlled microstructure may provide optimal porosity and microcracking during first carbonization so that the structure is amenable to effective and improved densification translating to higher mechanical properties. To design the material for effective densification, it becomes important to study the microstructure evolution during the earlier processing stages, namely as-cured and carbonized.

In this work, we studied the first two stages of CCC processing, namely as-cured and first-carbonization. Specimens with 0%, 2% and 5% (by weight of resin

precursor) CNFs and reinforcing carbon fabric treated with 0%, 12.5%, and 50% (by weight of acetone solvent) concentration of surfactant were processed to study the microstructure evolution and resulting ILSS properties at these two stages.

2. EXPERIMENTAL

2.1. Materials

Resole type phenolic resin, GP® 849D98/GP® 4824HB (supplier: Georgia-Pacific Resins, Inc.), was used as matrix precursor. Plain weave carbon fabric (supplier: US composites), Cat No. FG-CF10725, having a tow size of 6K and thickness 0.44 mm (0.017″) was used as reinforcement. The fabric was treated with Triton X-100 (*tert*-octylphenoxypolyethoxyethanol) surfactant (supplier: Sigma-Aldrich), the chemical structure of which is shown in Fig. 2. Commercial grade acetone was used for fabric desizing. PYROGRAF III- PR-24-PS type CNFs (supplier: Applied Sciences Inc., Ohio) having diameter of 60 to 150 nm and length of 30 to 100 μm were used for matrix modification.

2.2. Processing

Eight layers of C-fabric were cut to dimensions of 12.7 cm by 15.24 cm and the pieces were immersed in an acetone bath for five hours for desizing. The cycle was repeated over three times. Following the desizing and drying, the fabric layers were subjected to surfactant treatment. Three different concentrations of surfactant were prepared. In terms of surfactant: acetone solution these concentrations were 0%, 12.5%, and 50% surfactant by weight of acetone. For surfactant treatment, the plies were immersed in the surfactant-acetone solution for 24 h and the excess surfactant was soaked with blotting paper. Finally, the plies were heated at 70°C for one hour to remove all traces of acetone. Three variations were considered within the resin system, i.e. CNFs were manually mixed with phenolic resin in ratios of 0%, 2%, and 5% wt/wt respectively. The mixing was accomplished with a flat-faced wooden stick and was conducted for at least an hour. Catalyst was added to the resin-CNF mixture maintaining a resin-to-catalyst ratio of 100:8. Eight layers of C-fabric were wetted with resin using a hand-layup process followed by vacuum bagging to obtain uniform consolidation. The specimens were cured under vacuum for 24 h at ambient temperature (70°F), following which all specimens were post-cured in

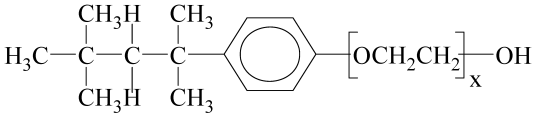

x = 9-10

Figure 2. Chemical structure of the Triton X-100 surfactant.

an oven at 70°C for 1 h. Specimens were subjected to carbonization process. The carbonization was conducted according to the following scheme:

(i) Stabilization (Muffle Furnace): the temperature was increased from 25°C to 200°C @ 25°C/h; dwell at 200°C for 2 h; cool down to 25°C.

(ii) Carbonization under nitrogen atmosphere (Tube Furnace): the temperature was increased from 25°C to 900°C at 240°C/h; dwell at 900°C for 5 h.

(iii) Cooling (Tube Furnace): the temperature was decreased from 900°C to 25°C at 240°C/h.

2.3. Testing

The interlaminar shear strength (ILSS) was determined by ASTM D 2344. The specimen dimensions were 18 mm × 6 mm × 3 mm. The span length was 12 mm. The cross-head movement rate was 1 mm/min. For each sample set, three (in some cases more than three) specimens were tested. The three-point bend short beam interlaminar shear strength (SBSS) was calculated by equation (1).

$$\tau^{\text{sbs}} = 0.75 \times \frac{P_{\text{m}}}{b \times h}, \tag{1}$$

where τ^{sbs} is the short beam shear strength (MPa), P_{m} is the maximum load observed during the test (N), b is the measured specimen width (mm), and h is the measured specimen thickness (mm).

A Philips SEM (Model 515) equipped with an energy dispersive spectrometer (EDS) was used for the microstructural analysis. To avoid any extra processing steps, the specimens were directly mounted on a metallic stub with a carbon based adhesive. The specimens were sputter coated with a thin gold film to prevent the examined region from localized charging and heating.

Pore area quantification from scanning electron microscopy (SEM) images was done using Image-Pro® Plus software (Media Cybernetics, Inc.). Figure 3 shows an example of the calculation of percentage pore area for a typical composite. Figure 3a represents the original SEM image, and Fig. 3b shows the pore area measured using the manual tracing feature of the software by the software. The percentage pore area was calculated dividing the total area by the pore area (obtained from Fig. 3b).

A Mettler Toledo instrument (Model AG204, equipped with an immersion density apparatus) was used for determining the physical properties (e.g. porosity and bulk density) of the composite at various stages of processing. The ASTM C 20 method was used as the reference standard.

For each sample set, four specimens were tested. The ASTM C 20 method calls for several steps to ensure that the test is valid for a certain type of material, namely; (i) specimens are not attacked by water; (ii) specimens are fully impregnated with water during boiling; (iii) blotting of saturated test specimens is performed in a consistent and uniform manner to avoid drawing water from pores; and (iv) 1 cm^3

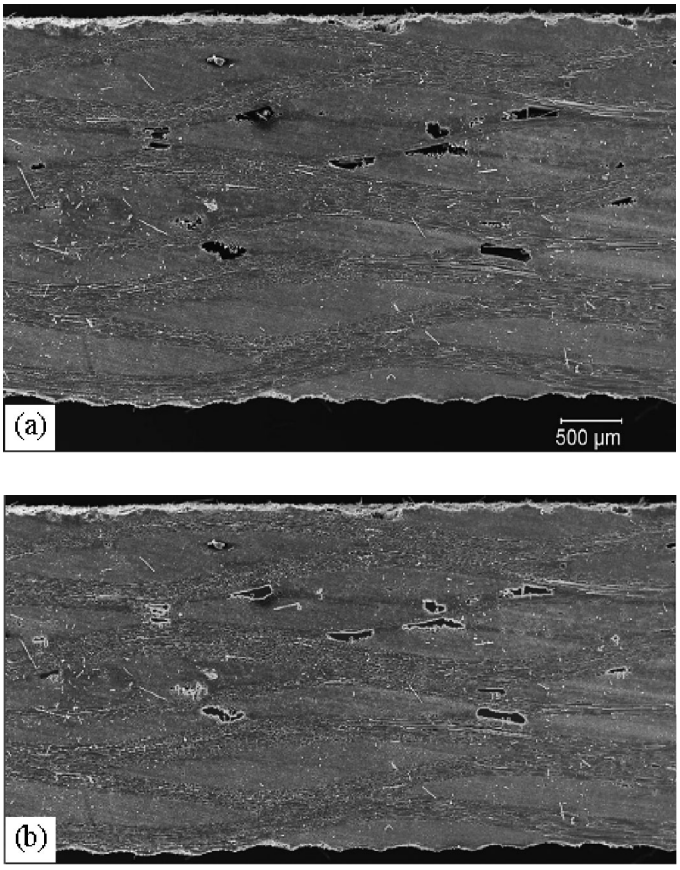

Figure 3. SEM image of a composite sample showing (a) the original image; (b) pore area quantified using the software.

of water (distilled) weighs 1 g. The testing starts with saturating the specimens with water. The following steps are taken to achieve the same; (i) place the specimen in boiling water for two hours (allowing no contact with the heated bottom of the container); and (ii) keep the specimen immersed in water (cold) for a minimum of 12 h. Though the image quantification method provides the pore area quantification of the transverse section, the porosity obtained using ASTM C 20 is a representative of the bulk composite.

3. RESULTS AND DISCUSSION

3.1. Effect of CNF addition on composite microstructure

3.1.1. As-cured composite. Figures 4a, 4b and 4c, represent SEM images for the 0%, 2% and 5% CNF specimens respectively. As indicated in the micrographs, porosity decreased with the addition of CNFs up to 2% CNF addition, beyond which

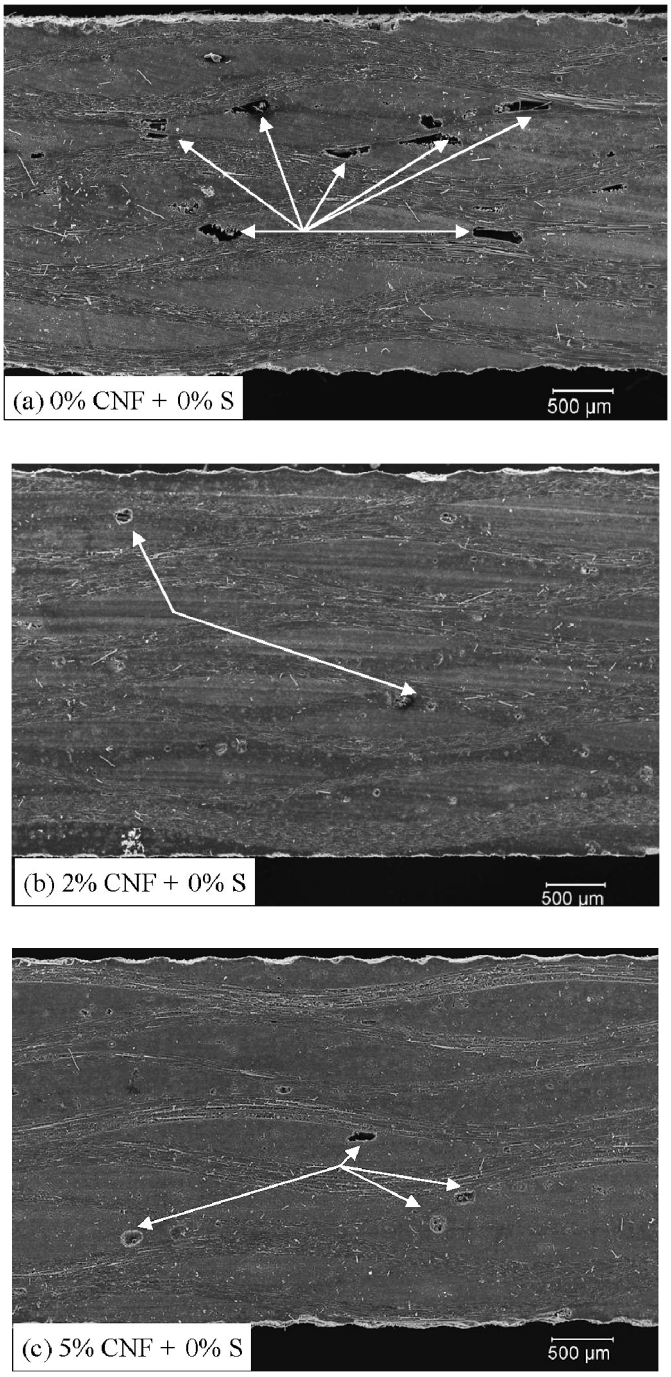

Figure 4. SEM images of uncarbonized (as-cured) samples for the (a) 0%, (b) 2% and (c) 5% CNF loading respectively (non-surfactant treated specimens) (Nomenclature: e.g. 2% CNF + 0% S means 2% CNF wt./wt. mixed resin and 0% surfactant treated fabric). The arrows show the presence and location of the pores.

the porosity increased (i.e. 5% CNF). This can be attributed to the decrease in curing shrinkage caused by the presence of CNFs, which acts as a filler. Furthermore, the tendency for agglomeration increases with increase in CNFs concentration. These agglomerates tend to create dry areas in the composite, which can lead to increased porosity. As a result of these two competing mechanisms (i.e. reduced shrinkage with CNFs addition and agglomeration of higher amount of CNFs), the specimens with 2% CNFs were found to have the least porosity. With increase in CNF concentration (5%), dry areas in the composite increased, which translated to higher porosity.

3.1.2. Carbonized composite. Figures 5a, 5b and 5c, represent SEM images for the 0%, 2% and 5% CNF specimens respectively. In comparison to the as-cured specimens, the carbonized specimens exhibited increase in porosity with increase in CNF addition. The increase in porosity for all carbonized specimens can be attributed to the volumetric thermal shrinkage of the resin precursor, and additional mechanism of interfacial debonding at the CNF/matrix as well as CNF/reinforcing fiber interfaces. It may be observed from Fig. 5a that a large delamination develops along the fabric/matrix interface for the 0% CNF specimens, with less distributed porosity. For the 2% (Fig. 5b) and 5% CNF specimens (Fig. 5c) there is higher overt porosity with equally spaced transverse matrix cracks; however, the interfaces between the fabric weave and the matrix are not prone to delamination, of the type observed for the 0% CNF (Fig. 5a) specimen.

3.2. Effect of surfactant treatment on composite microstructure

3.2.1. As-cured composite. Figures 6a, 6b and 6c, represent SEM images for the 0%, 12.5% and 50% surfactant treated specimens with 0% CNF loading respectively. It is evident that the least amount of porosity and delamination occurred in the 0% surfactant specimen. Figure 7 shows the presence of delaminations in the 50% surfactant treated specimen. Figures 8a, 8b and 8c are highly magnified images of the 0%, 12.5%, and 50% surfactant treated specimens respectively. It may be observed that the resin in 50% surfactant treated specimens has not fully cross-linked (as it resembles a plasticated region), though both 0% and 12.5% surfactant treated specimens appear to be fully cross-linked.

3.2.2. Carbonized composite. Figures 9a, 9b and 9c, represent SEM images for the 0%, 12.5% and 50% surfactant treated specimens with 0% CNF loading respectively. Separation of layers and pore formation at the weave crossings were observed to increase with increase in surfactant content. Figures 10a, 10b and 10c, represent magnified SEM images for the same specimens as in Figs 9a, 9b and 9c. It is clear from the micrographs that the matrix adhesion or the C-yield decreases with increase in surfactant content. The surfactant reduces the fiber/matrix interaction, thereby increasing porosity of the specimens after carbonization. Although this

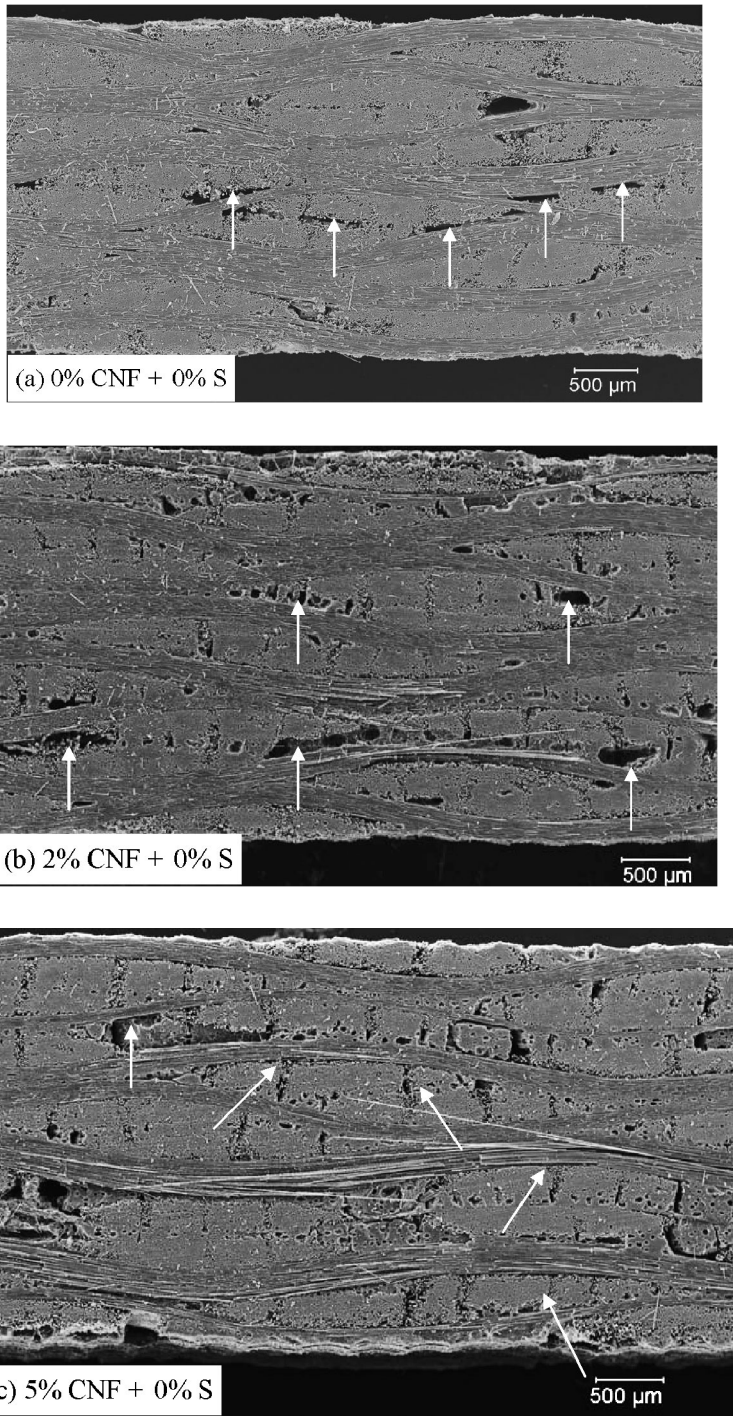

Figure 5. SEM images of carbonized samples for the (a) 0%, (b) 2% and (c) 5% CNF loading respectively (non-surfactant treated specimens).

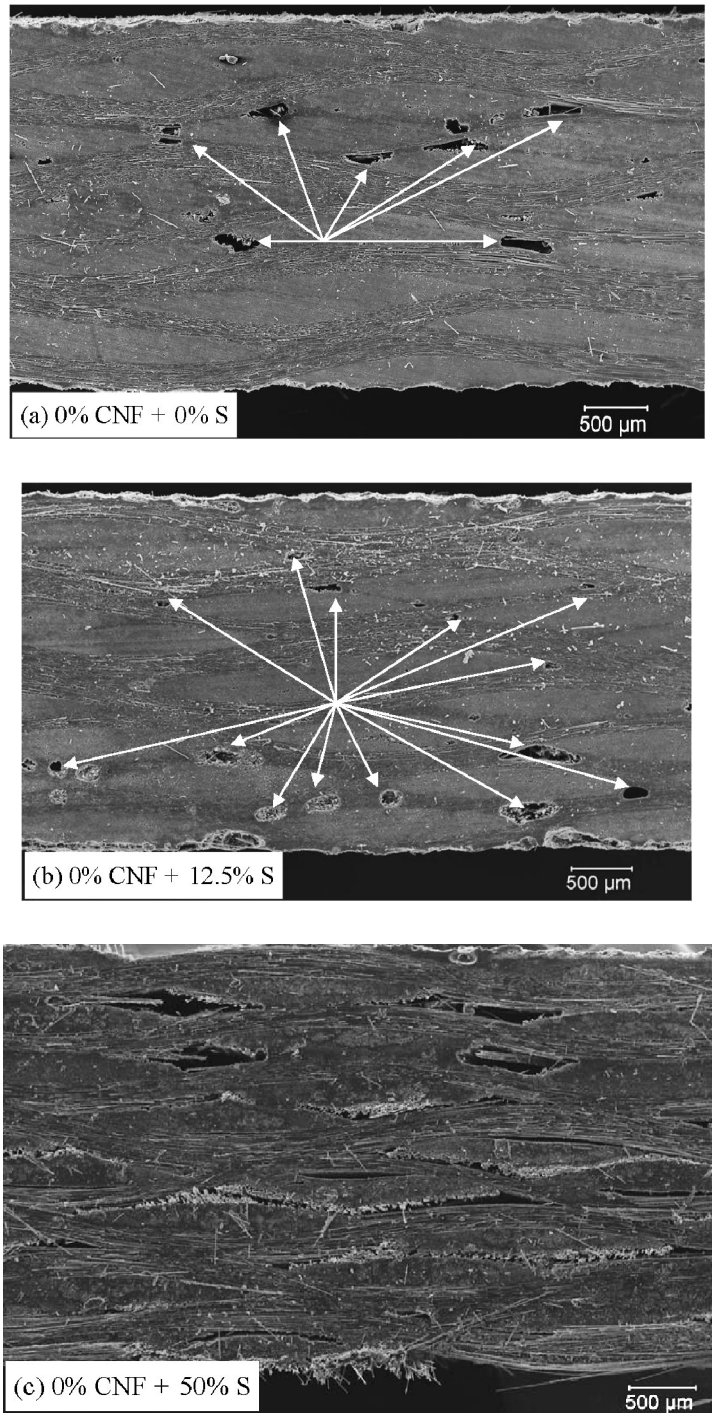

Figure 6. SEM images of uncarbonized samples for the (a) 0%, (b) 12.5% and (c) 50% surfactant treated specimens respectively having 0% CNF loading.

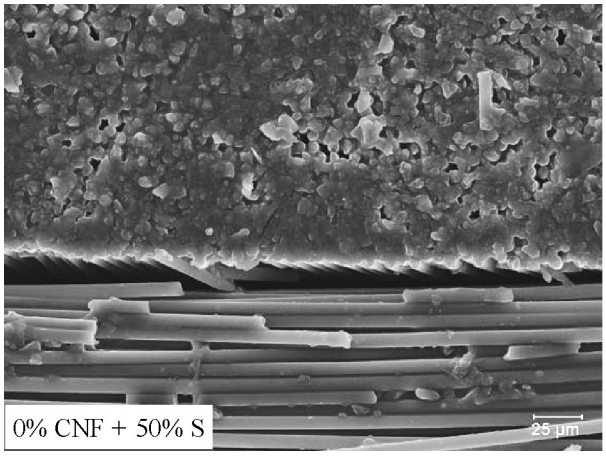

Figure 7. Highly magnified SEM image of 50% surfactant treated sample in the uncarbonized condition (with 0% CNF loading) showing clear delamination.

appears detrimental at the first-carbonization stage, the increase in open porosity is a desirable feature because it would enhance the infiltration of the densifying resin in subsequent processing.

3.2.3. Surfactant behavior during curing and carbonization of composite. Due to the inert nature of the C-fiber surface and absence of any chemical reaction, there is no covalent bonding between the surfactant molecules and the C-fiber. The carbonization of the surfactant is similar to carbonization of aliphatic hydrocarbons. During carbonization, rupturing of the C−H bonds takes place; the molecules also might go through mesophase (around 400°C), breaking the main chain and generating char. Furthermore, in absence of any binding force on the surfactant molecules, the C-yield becomes very low. The limited role of surfactant in the cross-linking leads to additional voids and cracks in the structure after carbonization. The −OH groups present at the end of surfactant can react with the functional sites present on the resole that take part in the cross-linking. This leads to reduction in cross-link density and hence more void formation in the carbonized structure. The reduction in ILSS and increase in voids percentage with increase in surfactant content (observed via SEM) verified this hypothesis.

3.3. Effect of CNF addition on microstructure of surfactant treated specimens

3.3.1. As-cured composite. Figures 11a, 11b and 11c represent SEM images for the 12.5% surfactant treated specimens with 0%, 2% and 5% CNF respectively. The porosity and void content were found to decrease with CNF addition up to 2% CNF. The 2% CNF specimens showed the minimum porosity. The porosity and void content increases at higher CNF loading, i.e. 5% CNFs. In the case of the 50% surfactant treated specimens, the trends were more uncertain. As previously

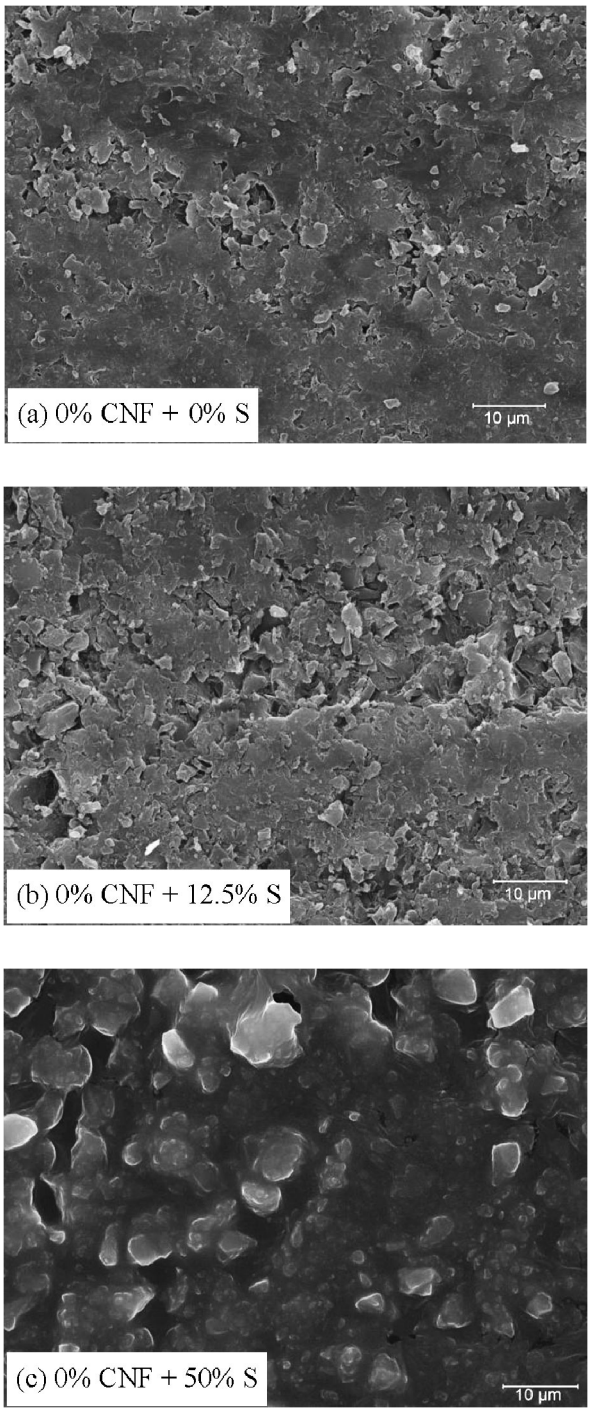

Figure 8. Magnified SEM images of uncarbonized samples for the (a) 0%, (b) 12.5% and (c) 50% surfactant treated specimens respectively having 0% CNF loading.

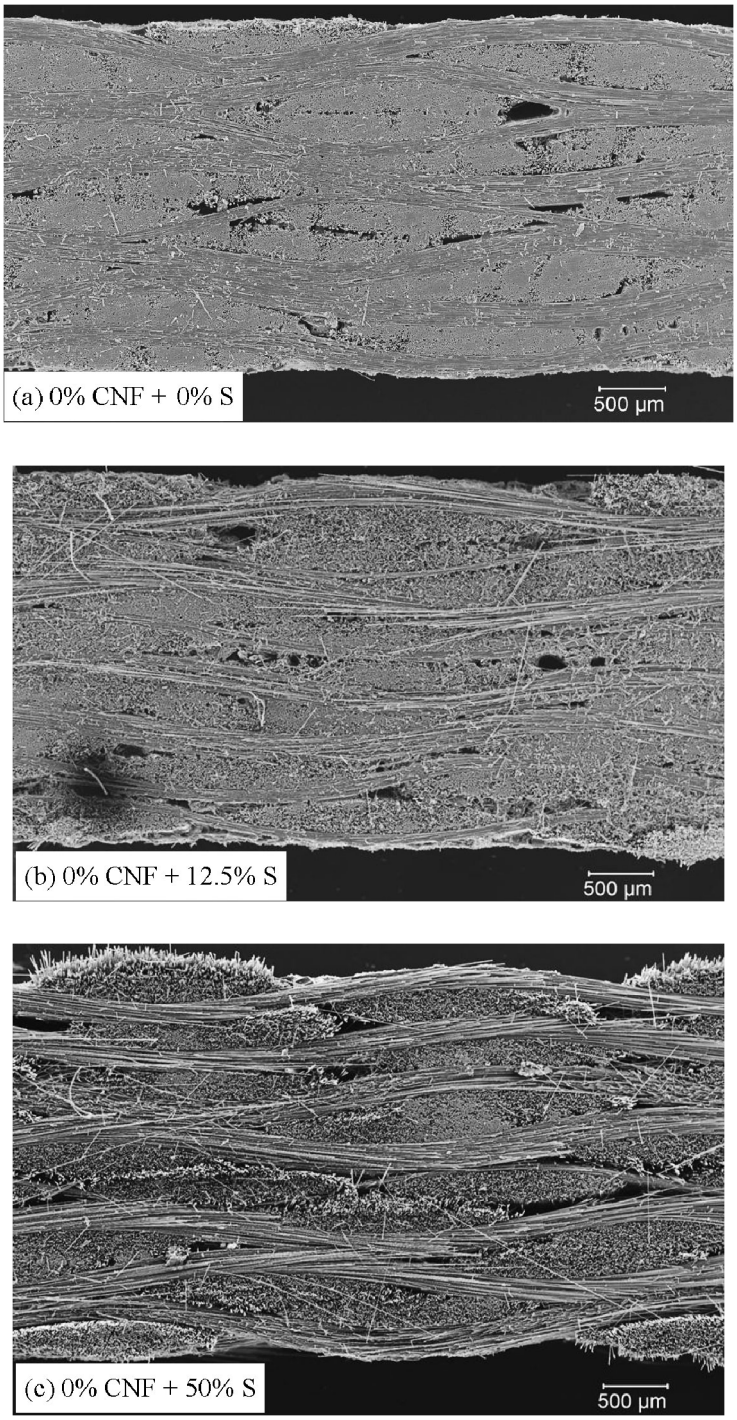

Figure 9. SEM images of carbonized samples for the (a) 0%, (b) 12.5% and (c) 50% surfactant treated specimens respectively having 0% CNF loading.

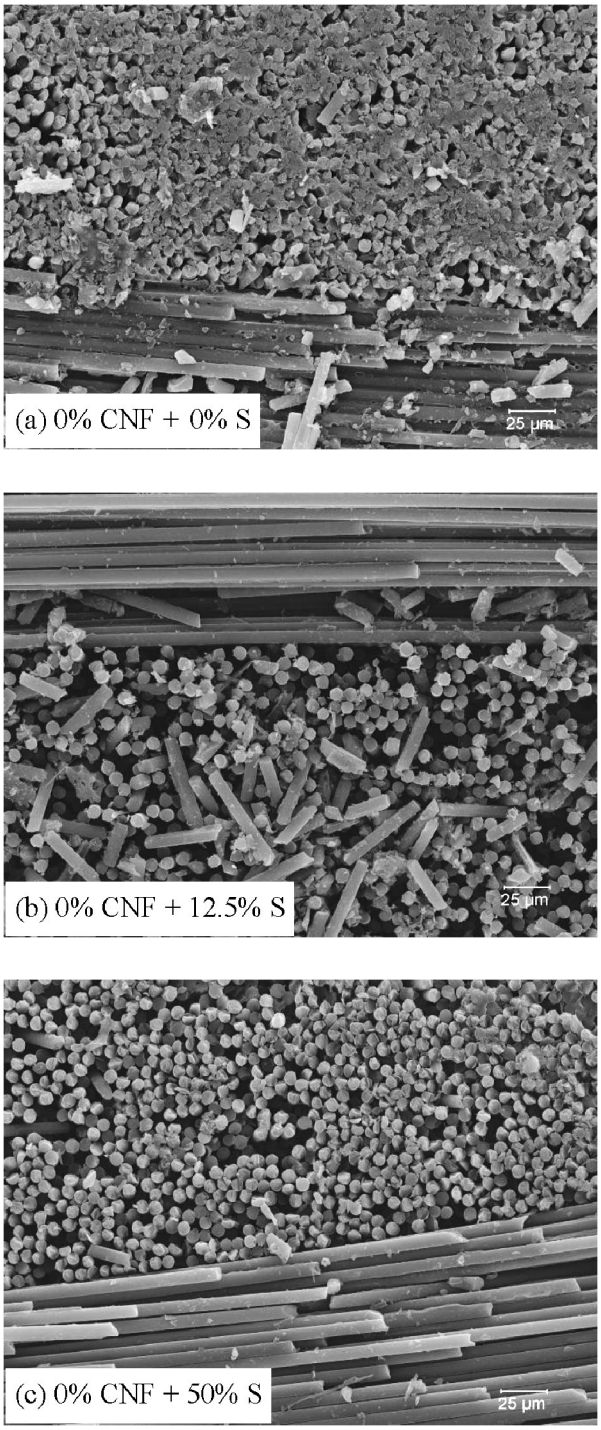

Figure 10. Magnified SEM images of carbonized samples for the (a) 0%, (b) 12.5% and (c) 50% surfactant treated samples respectively having 0% CNF loading.

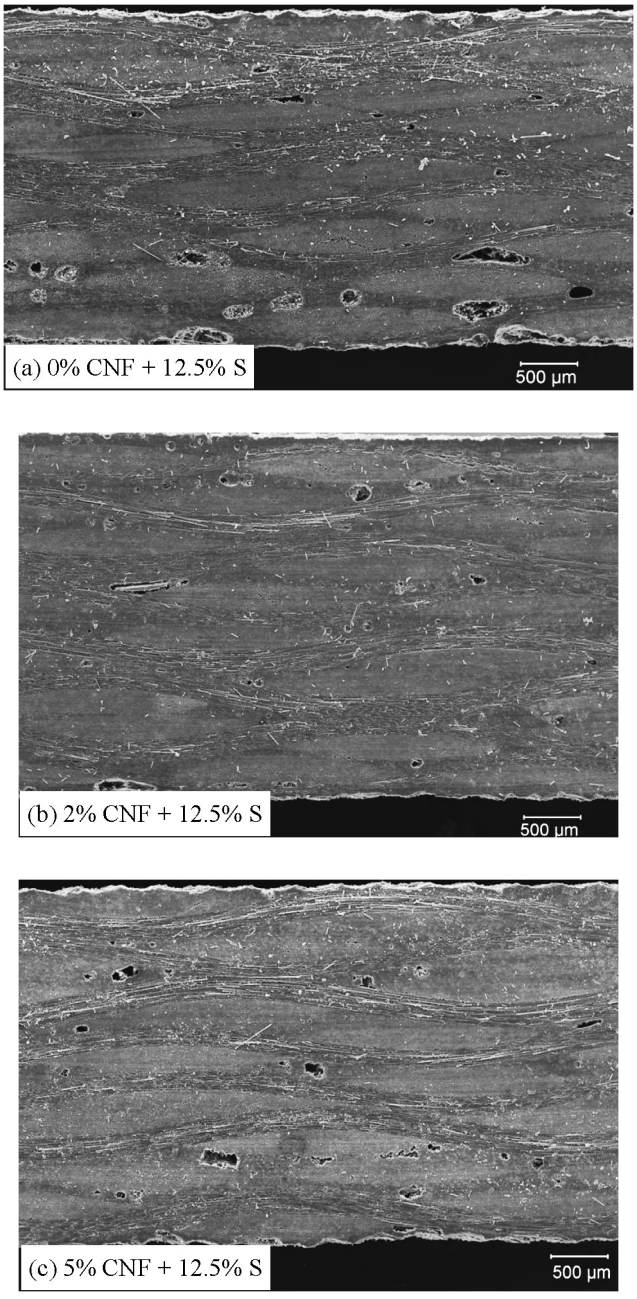

Figure 11. SEM images of 12.5% surfactant treated uncarbonized (as-cured) samples for the (a) 0%, (b) 2% and (c) 5% CNF loading respectively.

discussed, the 50% surfactant treated specimens inhibited full cross-linking and this is manifested in their behavior for the CNFs containing specimens. Figures

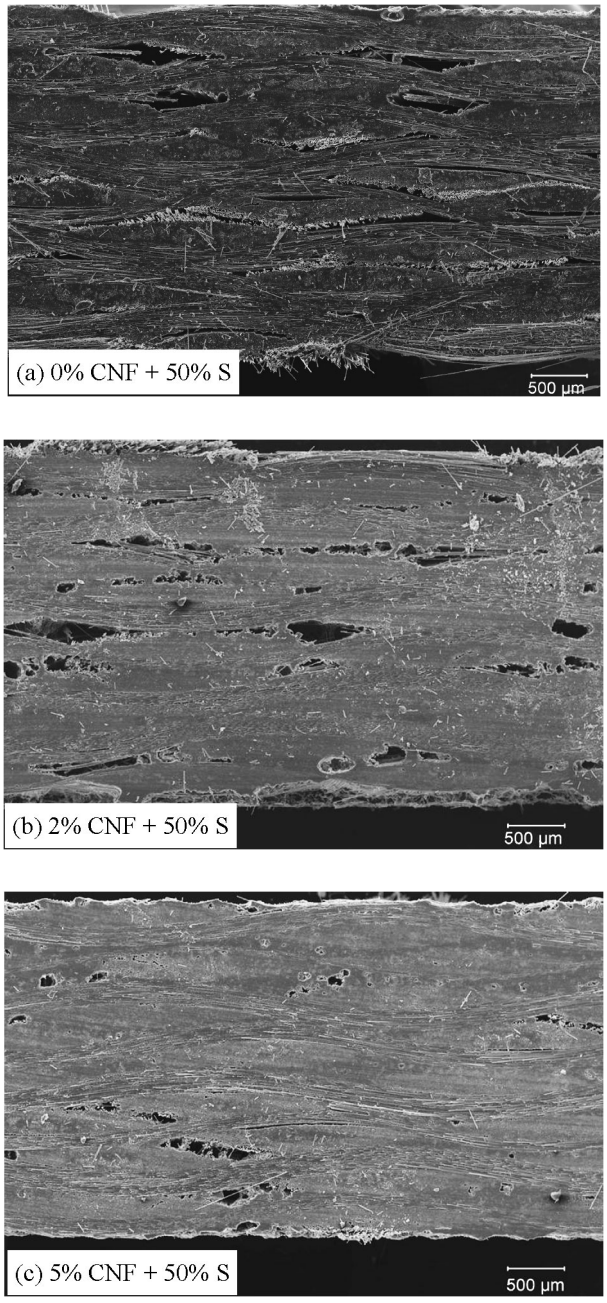

Figure 12. SEM images of 50% surfactant treated uncarbonized (as-cured) samples for the (a) 0%, (b) 2% and (c) 5% CNF loading respectively.

12a, 12b and 12c represent SEM images for the 50% surfactant treated specimens with 0%, 2% and 5% CNF respectively. Here it may be observed that the extent

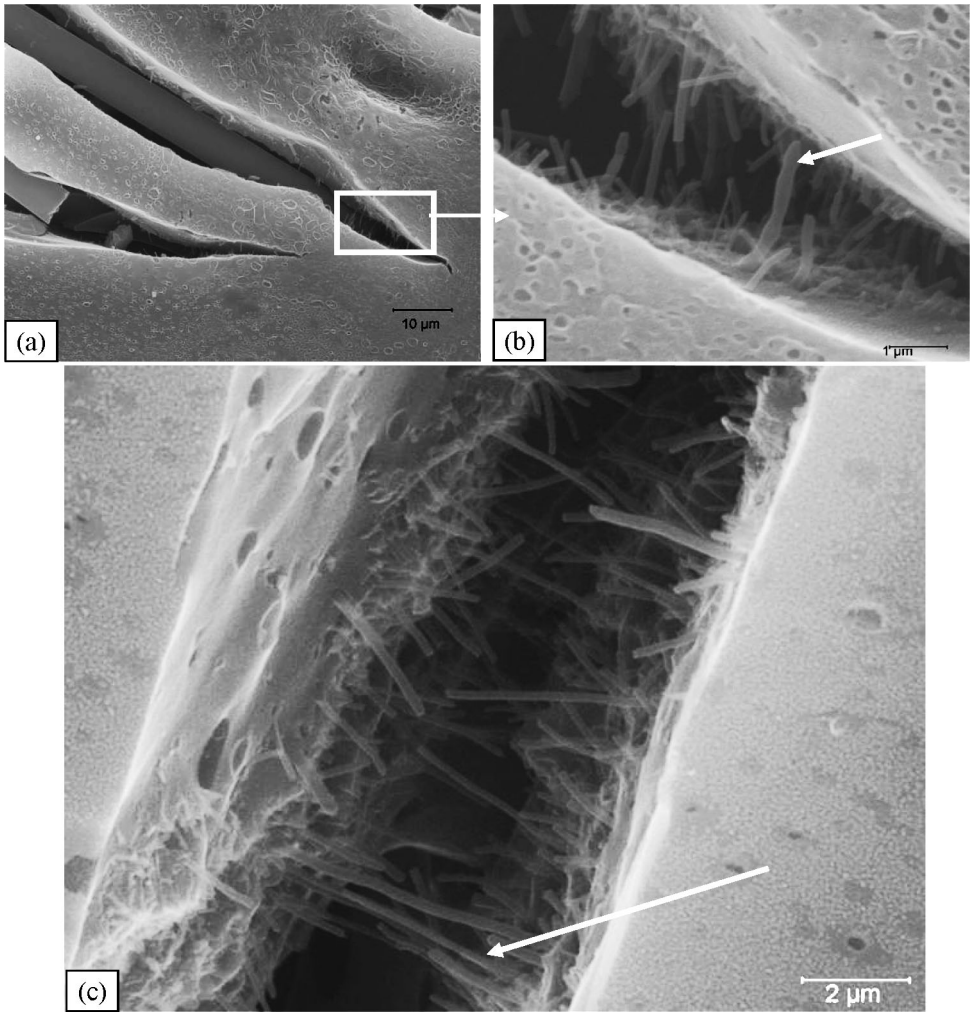

Figure 13. CNFs bridging the microcracks in a CCC; (a) microcrack image with low magnification; (b) magnified image of Fig. 12a showing the microcrack bridging with CNFs; (c) CNFs bridging the microcracks in another sample.

of delaminations, pores and voids reduces with increasing CNF percentage, i.e. from 0% to 5% CNFs. This may be explained as follows. The 50% surfactant inherently creates a weakly cross-linked structure. The CNFs have additional free volume within the microstructure to bridge the weaker interfaces and occupy weakly bonded regions. An evidence of microcrack bridging by CNFs is shown in Fig. 13. Hence, the higher the CNF percentage (such as the 5% CNF), the greater is the resistance to delamination. In other words, for the surfactant treated specimens, as the CNF concentration increases, delaminations and voids between various layers decrease. This can also be observed from the magnified micrographs, i.e. Figs 14a, 14b and 14c.

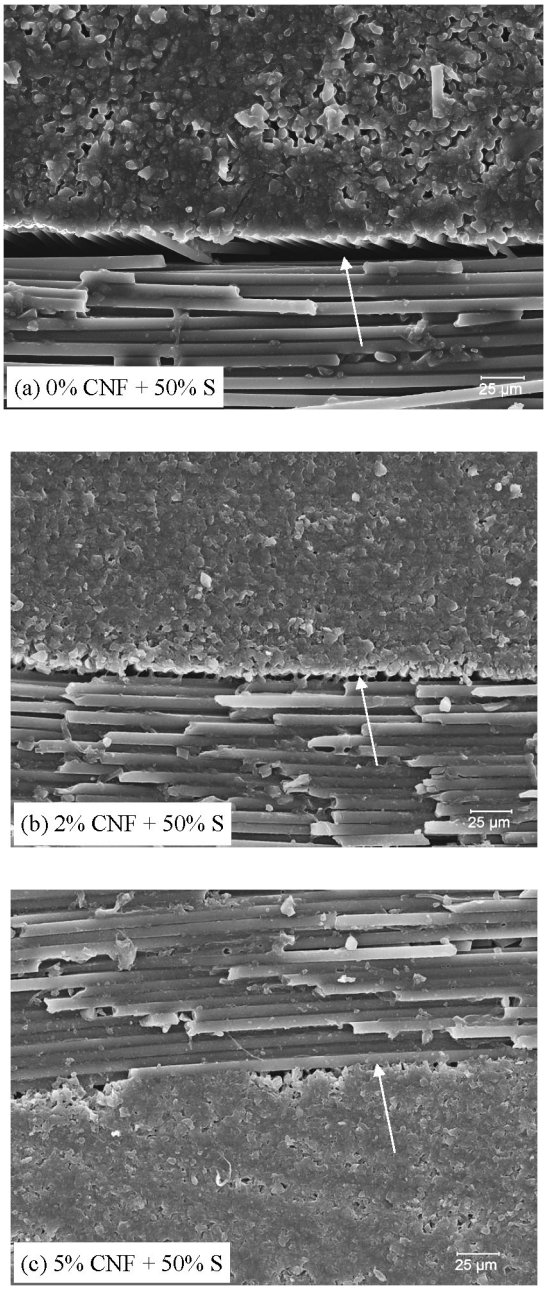

Figure 14. Magnified SEM images of 50% surfactant treated uncarbonized (as-cured) sample for the (a) 0%, (b) 2% and (c) 5% CNF loading respectively.

3.3.2. Carbonized composite. The trends observed for the carbonized specimens exhibited similar trend to the as-cured specimens. Figures 15a, 15b and 15c represent SEM images for 12.5% surfactant treated carbonized specimens with

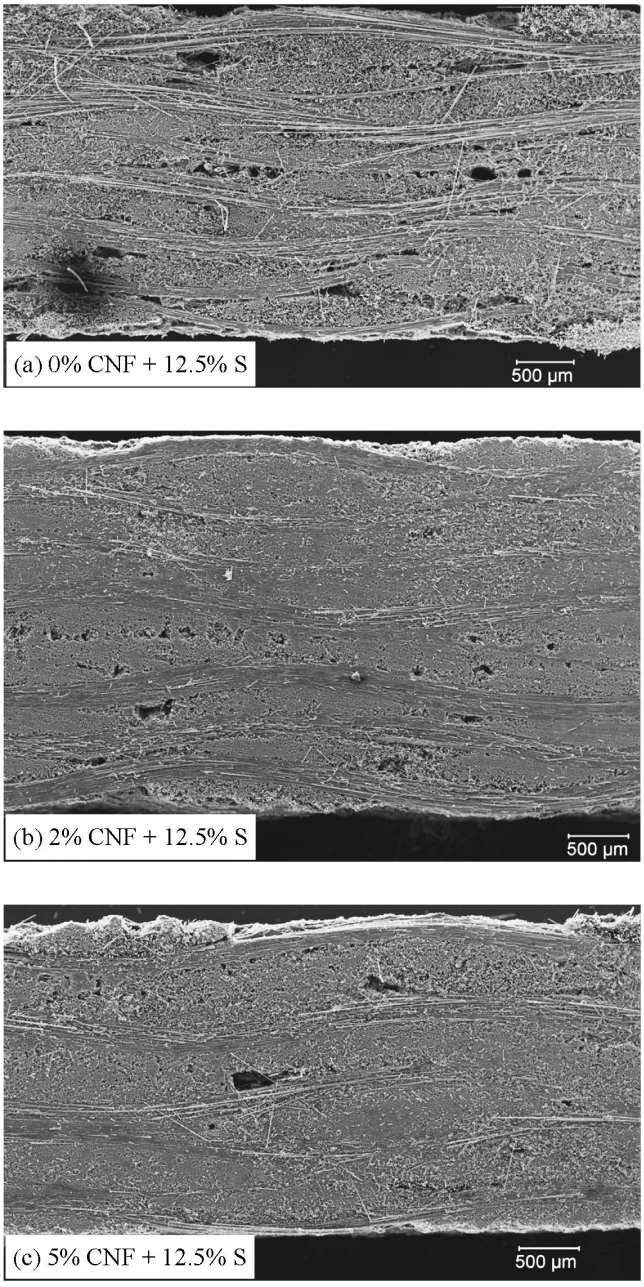

Figure 15. SEM images of 12.5% surfactant treated carbonized samples for the (a) 0%, (b) 2% and (c) 5% CNF loading respectively.

0%, 2% and 5% CNF, respectively. More delaminations and voids were observed in the 0% CNF specimens. Delaminations and voids were found to decrease with increasing percentage of CNFs. Similar observations were recorded for the 50% surfactant treated specimens with 0%, 2% and 5% CNF (Figs 16a, b and c respectively).

3.4. Porosity quantification

Porosity of a composite is directly or indirectly related to many other properties such as the strength, permeation of gases and liquids, electrical and thermal conductivity, opacity, and chemical reactivity. Porosity affects other physical properties, such as water absorption, specific gravity, and bulk density. In this work, porosity has been quantified using two methods, namely; image analysis from the SEM micrographs (using Image-Pro® Plus software by Media Cybernetics, Inc.) and ASTM C 20. The results presented in Sections 3.4.1 and 3.4.2 are based on the porosity measured from image analysis. Results in Section 3.5.1 are based upon ASTM C 20.

3.4.1. Porosity quantification of the as-cured composite. The SEM images of both as-cured and carbonized composite were analyzed using the image analysis software. Figure 17 compares the porosity results for the as-cured specimens with various surfactant treatments and CNF loading. Porosity was found to decrease with the addition of CNFs (the only exception to this trend was the 50% S sample set). In the case of no surfactant treatment, 2% CNF specimens showed the minimum porosity (pore area of 0.08% as compared to 0% CNF which showed the maximum pore area of 1.41%). For 12.5% surfactant treated specimens, the 2% CNF specimen showed the minimum pore area of 0.26% and 0% CNF specimen showed the maximum pore area of 1.35%. On an average, for a particular percentage of CNF loading, porosity was found to increase with increase in surfactant content in the fabric treatment. This is attributed to the improper wetting of C-fiber with resin in the case of increasing surfactant treatment.

3.4.2. Porosity quantification of the carbonized composite. Figure 18 compares the porosity results obtained for the carbonized specimens. Porosity was found to decrease with the addition of CNFs (except 0% S). In the case of no surfactant treatment (0% S), porosity increased with the addition of CNFs (pore areas were 2.2, 4.2 and 4.43% for 0, 2 and 5% CNF loadings respectively). This can also be observed from the SEM micrographs shown in Section 3.1.2. For 12.5% surfactant treated specimens, 2% and 5% CNF loaded specimens showed the comparable pore area of approximately 0.75%, but 0% CNF loaded specimen showed the pore area of 2.55%. For 50% surfactant treated specimens, pore area decreased with the increasing percentage of CNF in the loading. The pore area values were 5.63, 3.27 and 0.95% for 0, 2 and 5% CNF loadings respectively.

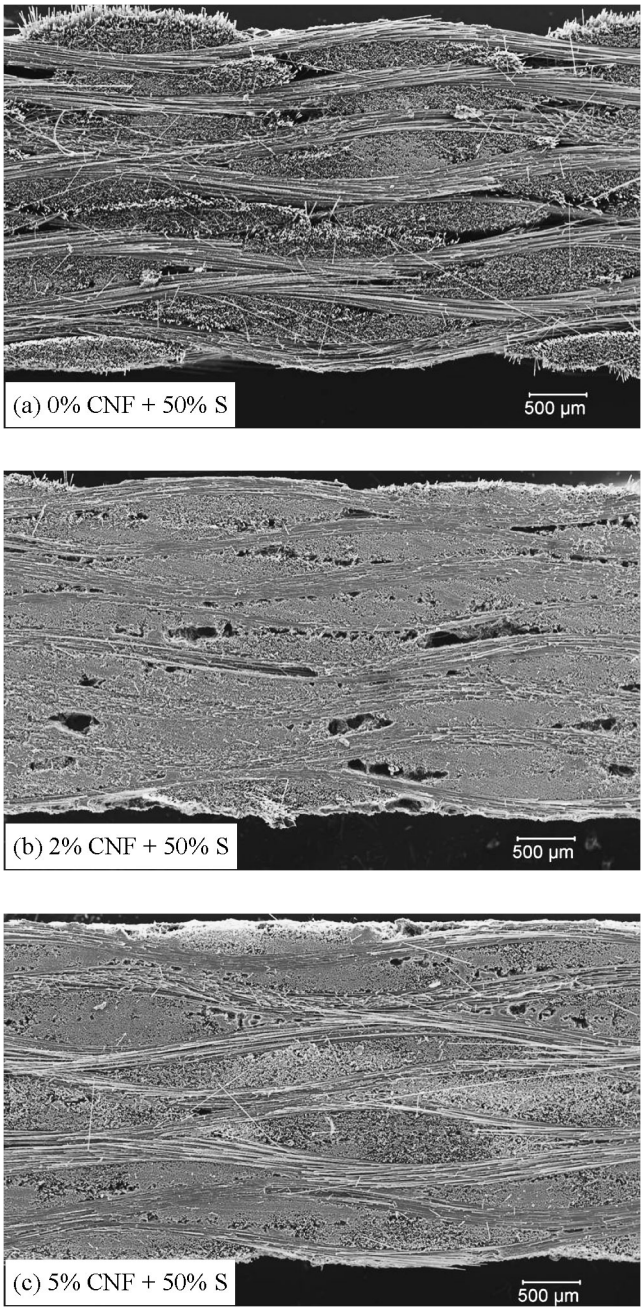

Figure 16. SEM images of 50% surfactant treated carbonized samples for the (a) 0%, (b) 2% and (c) 5% CNF loading respectively.

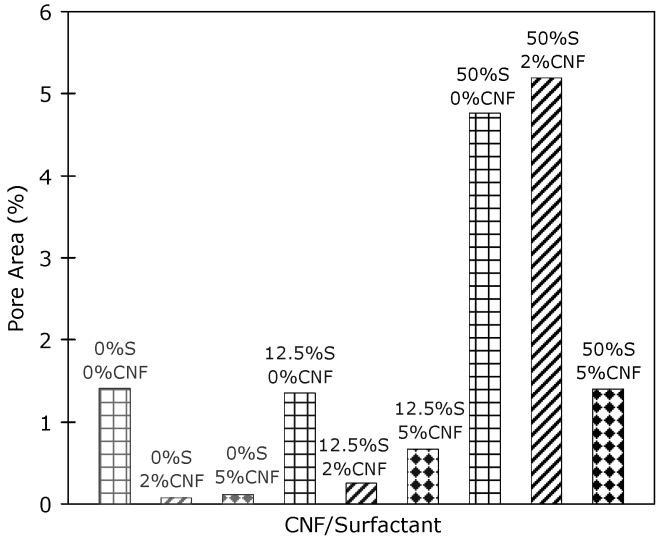

Figure 17. Effect of different percentages of CNF loading and surfactant treatment on the pore area of as-cured composite as measured from SEM images using an image analysis software.

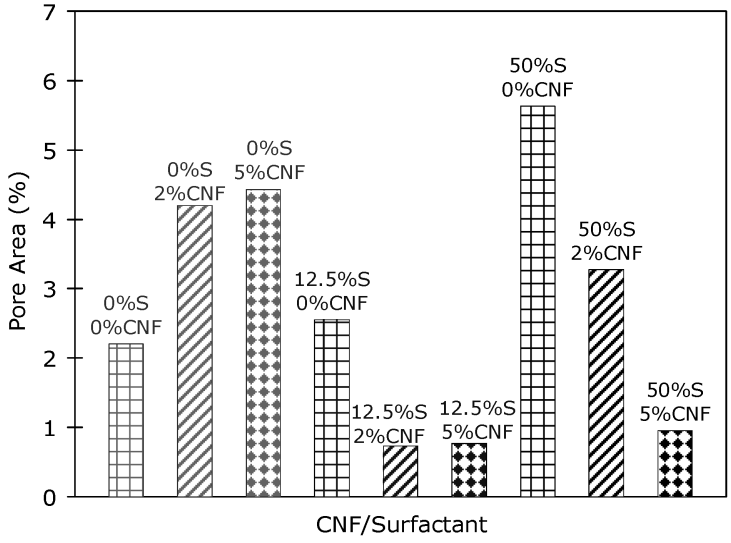

Figure 18. Effect of different percentages of CNF loading and surfactant treatment on the pore area of carbonized composite as measured from SEM images using an image analysis software.

3.5. Porosity

Porosity, of the as-cured and carbonized composites was determined according to ASTM C 20. Figure 19 compares the effect of CNF loading and surfactant treatment on the porosity of as- cured and carbonized composite.

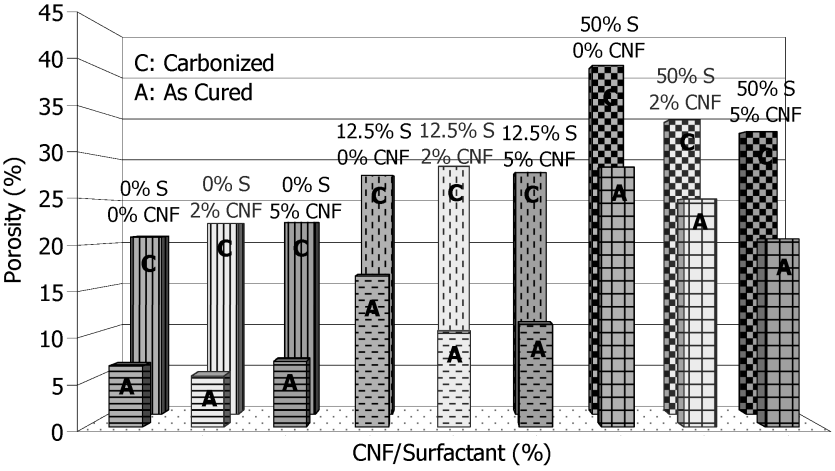

Figure 19. Effect of different percentages of CNF loading and surfactant treatment on the porosity of as-cured and carbonized composites.

3.5.1. Porosity of as-cured composites. The porosity measured by ASTM C 20 agreed well with the trends observed from SEM images. As shown in Fig. 19, 2% CNF specimens showed the minimum porosity. Both 0% and 5% CNF specimens showed comparable porosity (approx. 7%). For a particular percentage of CNF, porosity increased with increase in surfactant content (increased porosity and interlayer separation with increase in surfactant percentage was also evident in SEM studies, Section 3.2.1). For non-CNF specimens, porosity increased from 6.7% to 16.6% to 28.5% for 0, 12.5 and 50% surfactant treatment respectively. For 50% surfactant, porosity decreased with increase in CNF % (values were 28.5%, 25%, 20.1% for 0, 2 and 5% CNF loadings respectively).

3.5.2. Porosity of carbonized composites. Generation of voids and cracks during carbonization leads to free spaces in the composite. This is evident from the Fig. 19 which shows significant increase in porosity after carbonization. On an average, the carbonized composite showed 16% increase in porosity as compared to the as-cured composite. For both 0% and 12.5% surfactant treatment, CNF containing specimens showed higher porosity. For a particular percentage of CNFs, porosity increased with increase in surfactant percent treatment. For 0% surfactant treatment, the 2% CNF and 5% CNF specimens showed comparable porosity. For 50% surfactant, porosity decreased with increase in CNF. Increase in porosity with increase in surfactant content was found to decrease with increase in CNF content (When the surfactant percentage increased from 0% to 50% treatment; porosity of 0% CNF specimens increased from 20.7% to 40.8%, porosity of 2% CNF specimens increased from 22.3% to 34.3%, and porosity of 5% CNF specimens increased from 22.4% to 33%).

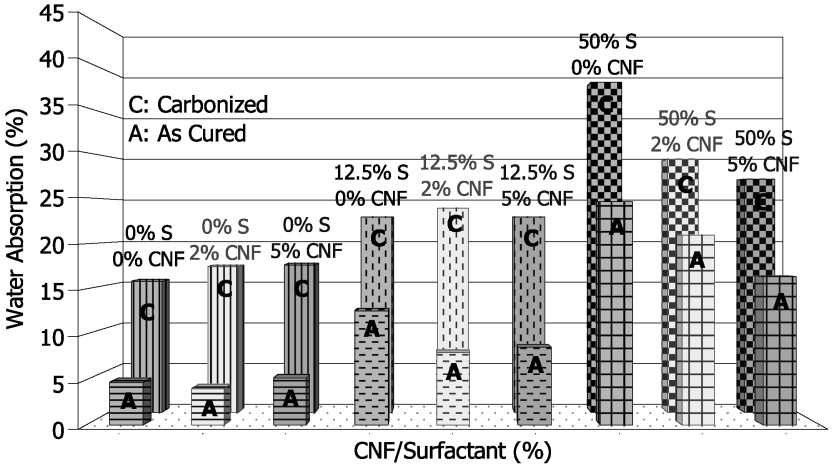

Figure 20. Effect of different percentages of CNF loading and surfactant treatment on the water absorption of as-cured and carbonized composite.

3.6. Interlaminar shear strength (ILSS)

3.6.1. ILSS of as-cured composite. The ILSS of both as-cured and carbonized composite was determined according to ASTM D 2344. The standard deviation for each ILSS value is shown as the error bars. Figure 20 summarizes the ILSS results obtained for the as-cured specimens. The ILSS was significantly influenced by the surfactant and CNFs. Higher ILSS values were exhibited by the specimens that were not treated with the surfactant (0% surfactant). The untreated specimens (i.e. 0% surfactant, 0% CNF) exhibited an average ILSS of 36 MPa. The addition of 2% CNFs improved the ILSS values by 14% (from 35.27 MPa to 40.28 MPa) as compared to the 0% CNF specimens. The 5% CNFs specimens exhibited 7% lower values (32.7 MPa) of ILSS over the 0% CNF specimens (35.27 MPa). For a particular percentage of CNFs, the ILSS values were found to decrease with increasing amount of surfactant. This further confirmed that the fabric-resin interface weakens due to surfactant addition. The 50% surfactant treated specimens did not yield conclusive trends with respect to the CNF percentages, but their overall ILSS was greatly reduced by an average of 75% (from 36 MPa to 9 MPa) of the values obtained for 0% surfactant treated specimens.

3.6.2. ILSS of carbonized composite. Figure 21 summarizes the ILSS results obtained for the carbonized specimens. Significant decrease in the mechanical property of the composite was observed after first carbonization, as compared to the as-cured specimens. For the 0% surfactant carbonized specimens, the ILSS decreased by an average of 84% in comparison to its as-cured counterpart for all the three cases i.e., 0%, 2% and 5% CNFs. The ILSS trends observed for the 0% surfactant followed that of its as-cured stages, giving a maximum ILSS for 2% CNF

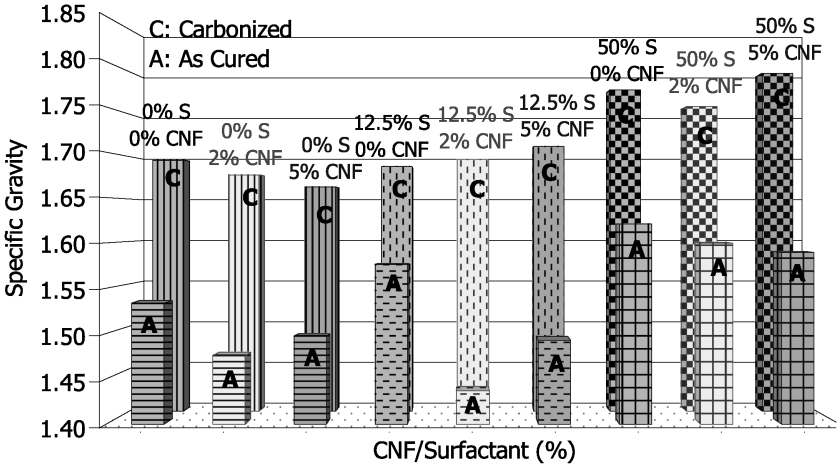

Figure 21. Effect of different percentages of CNF loading and surfactant treatment on the specific gravity of as-cured and carbonized composite.

(6 MPa). For a particular percentage of surfactant treatment, properties improved with CNFs addition.

3.6.3. Interpretations from the ILSS studies. The overall reduction in ILSS after first carbonization across all the specimens can be attributed to the void formation, micro-crack development, and micro de-bonds within the layers during carbonization. In addition, the interfacial contact between the fiber and the matrix decreases because the matrix tends to shrink away from the fiber during the carbonization. Since the CNFs are incompressible with respect to the matrix, they reduce shrinkage during carbonization. As the shrinkage is less, the matrix will not be as compact (i.e. the tendency to conform to minimum volume) and hence the propensity of weight loss through elemental carbon loss increases with increase in CNFs percentage, which translates to higher porosity. Surfactant treated specimens showed higher population of micro-cracks and delaminations after first carbonization. It was observed that, the CNFs tend to bridge the micro-cracks and delaminations as shown in Fig. 13. It is during the densification that open pores are filled with resin and microcraks get sealed. This leads to decrease in porosity of the composite and hence increase in ILSS of the composites after densification.

It should be understood that true/effective interlaminar area under stress is smaller than theoretical area because of the presence of voids or cracks in that area. The effect of voids on ILSS is also dependent on the position of voids. If the voids are near the neutral plane, the shear strength will be greatly affected. Voids near the outer surfaces will have minimum effect on the ILSS. This differential affect can be understood from the fact that shear stresses increase from zero to maximum from a surface to the neutral/mid-plane. Various researchers [26–31] have reported the correlation between ILSS and other physical properties. Figures 22 and 23 show a

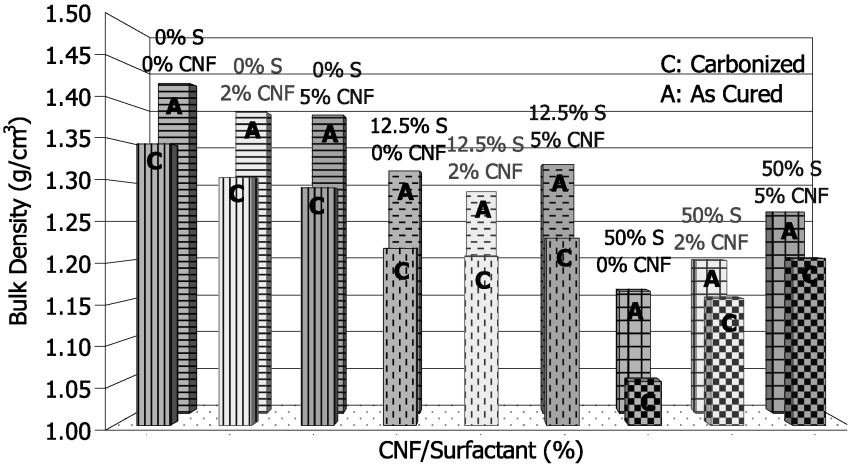

Figure 22. Effect of different percentages of CNF loading and surfactant treatment on the bulk density of as-cured and carbonized composite.

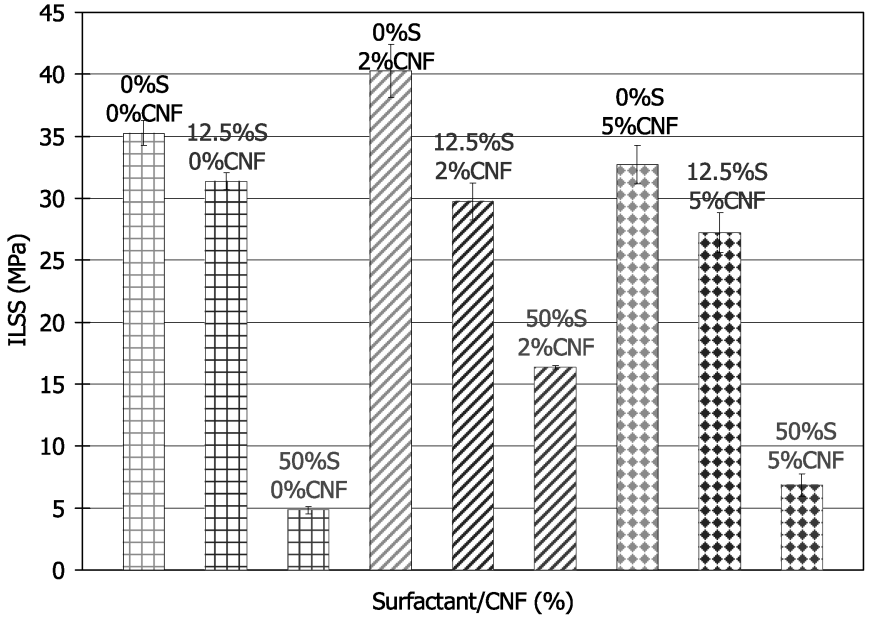

Figure 23. Interlaminar shear strength of as-cured samples.

linear decrease in ILSS with increase in porosity for the as-cured and carbonized composites respectively.

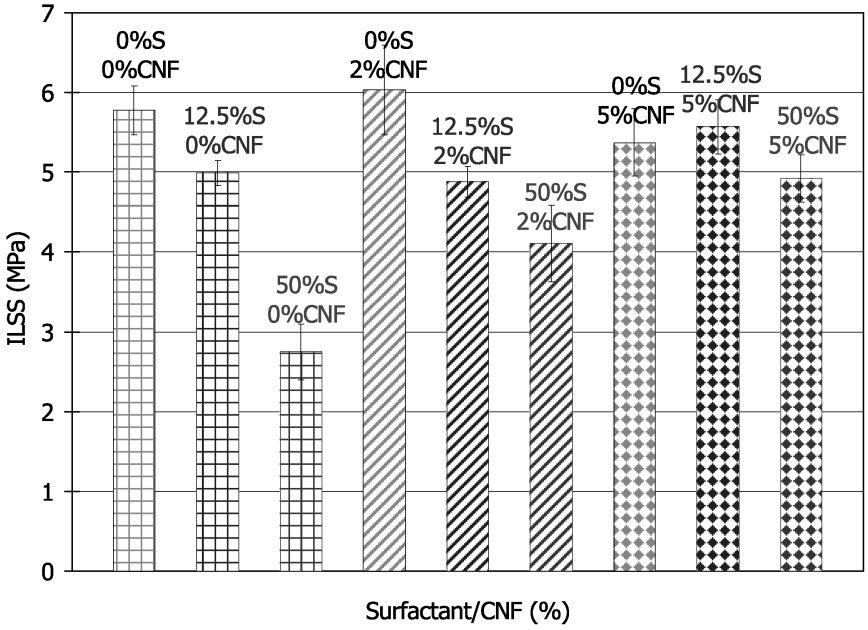

Figure 24. Interlaminar shear strength of carbonized samples.

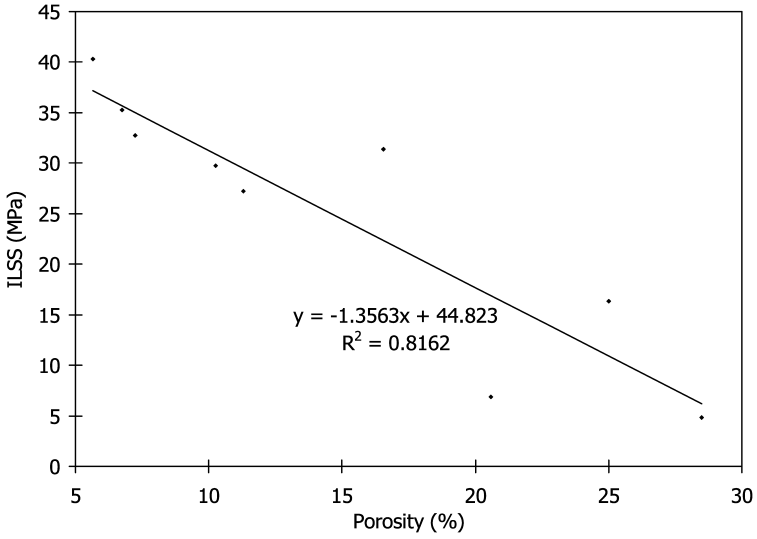

Figure 25. Decrease in ILSS with increase in porosity for as-cured composites.

4. CONCLUSIONS

The use of CNFs provides a bridging mechanism for matrix microcracking and reducing matrix shrinkage that occurs during first carbonization, thereby implying that delamination growth can be suppressed. The localized reinforcements offered

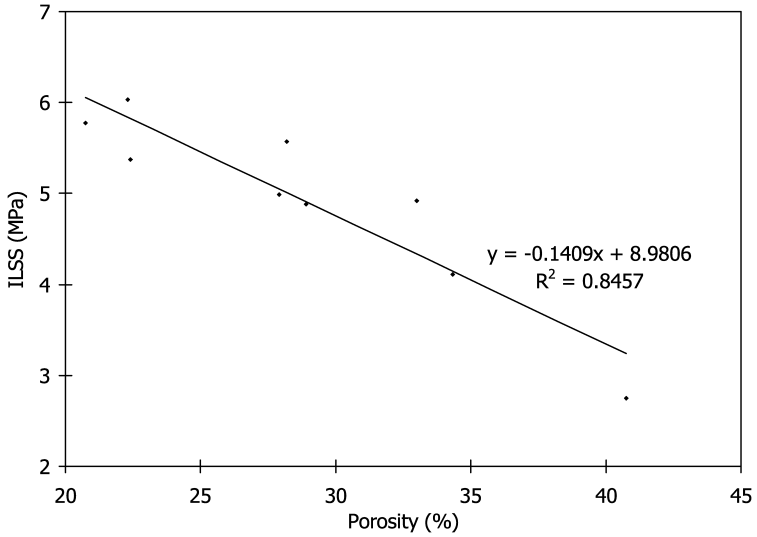

Figure 26. Decrease in ILSS with increase in porosity for carbonized composites.

by the CNFs reduce the overall matrix content in the composite, increasing percentage of graphitic carbon in the specimen. At the as-cured and first-carbonized stages, an optimal value of 2% CNFs yielded highest ILSS values of $\sim$ 40 MPa and 6 MPa, respectively. Surfactant treatment of the C-fabric adversely affected the interfacial properties, at both as-cured and carbonized stages. At the as-cured stage, the non-surfactant treated specimens, for 0% CNF loading, showed 12% and 631% higher ILSS values than the 12.5% and 50% surfactant treated specimens respectively. The surfactant treatment of the carbon fibers weakens the interface due to reduced cross-linking of the matrix in the resulting composite. As a result, porosity and debonding were found to increase with increase in surfactant percentage treatment of the carbon fabric. At both as-cured and carbonized stages of CCC processing, for a particular CNF percentage, porosity was found to increase with increase in surfactant percentage. Similarly, for a particular percentage of CNF loading, ILSS was found to decrease with increase in surfactant treatment at both as-cured and carbonized stages. An inverse linear trend between ILSS and porosity was observed for both as-cured and carbonized specimens. Further work is required to find the effect of CNF loading and surfactant treatment on further stages of the process, namely densification. Studies would also be conducted for determining the mode of failures (delamination, fracture, fracture concomitant with fiber–pullout, etc.) when CNFs are used.

Acknowledgement

Support provided by the United States Space Defense Missile Command is gratefully acknowledged.

REFERENCES

1. E. Fitzer, Carbon based composites, *J. Chimie Physique* **81**, 717–733 (1984).
2. E. Fitzer, The future of carbon-carbon composites, *Carbon* **25**, 163–190 (1987).
3. G. Savage, *Carbon-carbon Composites*, pp. 323–359, Chapman and Hall, London (1993).
4. F. Gao, J. W. Patrick and A. Walker, The characterization of cracks and voids in two-dimensional carbon-carbon composites, *Carbon* **31**, 103–108 (1993).
5. T. J. Kang and Y. W. Jeong, Mechanical properties of matrix-modified carbon/carbon composites, *Polym. Polym. Compos.* **5**, 469–475 (1997).
6. C. C. M. Ma, J. M. Lin, W. C. Chang and T. H. Ko, Carbon/carbon nanocomposites derived from phenolic resin–silica hybrid ceramers: microstructure, physical and morphological properties, *Carbon* **40**, 977–984 (2002).
7. E. Yasuda, Y. Tanabe, L. M. Manocha and S. Kimura, Matrix modification by graphite powder additives in carbon fiber/carbon composite with thermosetting resin precursor as a matrix, *Carbon* **26**, 225–227 (1988).
8. A. Y. C. Hung, F. Y. Wang, S. R. Yeh, W. J. Chen and C. C. Ma, Carbon/carbon composites derived from poly(ethylene oxide)-modified novolac-type phenolic resin: microstructure and physical, and morphological properties, *J. Appl. Polym. Sci.* **84**, 1609–1619 (2002).
9. J. M. Lin, C. C. M. Ma and W. C. Chang, Carbon/carbon composites derived from phenolic resin/silica hybrid ceramers, Part I: Oxidation resistance and morphological properties, *J. Mater. Sci.* **36**, 4259–4266 (2001).
10. M. Müller, K. M. Beinborn and K. J. Hüttinger, The significance of the fibre coating in the production of carbon fibre-reinforced carbons from HT carbon fibres and phenolic resin as matrix precursor: II. Phenolic resin coatings, *Carbon* **33**, 1043–1046 (1995).
11. R. J. Zaldivar, R. W. Kobayashi, G. S. Rellick and J. M. Yang, Carborane-catalyzed graphitization in polyarylacetylene-derived carbon-carbon composites, *Carbon* **29**, 1145–1153 (1991).
12. C. C. M. Ma, W. C. Chang and N. H. Tai, Effects of precursor thermal aging and fiber arrangement on the properties of carbon/carbon (C/C) composites, *Internat. Conf. Adv. Compos. Mater.*, pp. 1405–1409 (1993).
13. N. H. Tai, M. K. Yeh, C. H. Liu, H. M. Hsueh and C. H. Yang, Synthesis of carbon nanotubes and characterization of CNTs/phenolic composites, in: *Proc. 14th Internat. Conf. Compos. Mater. ICCM-14*, San Diego, CA, USA (2003).
14. S. S. Tzeng and Y. G. Chr, Evolution of microstructure and properties of phenolic resin-based carbon/carbon composites during pyrolysis, *Mater. Chem. Phys.* **73**, 162–169 (2002).
15. http://www.ml.afrl.af.mil/stories/mlb-00378.html (accessed Sept. 3, 2004).
16. http://www.wtec.org/loyola/nano/US.Review/09_03.htm (last accessed June 2006).
17. R. D. Patton, C. U. Pittman, L. Wang and J. R. Hill, Vapor grown carbon fiber composites with epoxy and poly(phenylene sulfide) matrices, *Composites Part A: Appl. Sci. Manufact.* **30**, 1081–1091 (1999).
18. J. Sandler, P. Werner, M. S. P. Shaffer, V. Demchuk, V. Altstadt and A. H. Windle, Carbon-nanofibre-reinforced poly(ether ether ketone) composites, *Composites Part A: Appl. Sci. Manufact.* **33**, 1033–1039 (2002).
19. K. Lozano, J. B. Rios and E. V. Barrera, A study on nanofiber-reinforced thermoplastic composites (II): investigation of the mixing rheology and conduction properties, *J. Appl. Polym. Sci.* **80**, 1162–1172 (2001).
20. G. C. Tibbetts and J. J. McHugh, Mechanical properties of vapor-grown carbon fiber composites with thermoplastic matrices, *J. Mater. Res.* **14**, 2871–2880 (1999).
21. C. V. Santos, A. L. M. Hernández, F. Fisher, R. Ruoff and V. M. Castaño, Dynamical mechanical and thermal analysis of carbon nanotube–methyl-ethyl-methacrylate nanocomposites, *J. Phys. D: Appl. Phys.* **36**, 1423–1428 (2003).

22. B. Vigolo, P. Launois, M. Lucas, S. Badaire, P. Bernier and P. Poulin, Fibers of carbon nanotubes, *Mater. Res. Soc. Sympos. Proc.* **706**, 3–8 (2002).
23. S. Bandow, A. M. Rao, K. A. Williams, A. Thess, R. E. Smalley and P. C. Eklund, Purification of single-wall carbon nanotubes by microfiltration, *J. Phys. Chem. B* **101**, 8839–8842 (1997).
24. X. Gong, J. Liu, S. Baskaran, R. D. Voise and J. S. Young, Surfactant-assisted processing of carbon nanotube/polymer composites, *Chem. Mater.* **12**, 1049–1052 (2000).
25. S. S. Ranta and C. E. Bakis, Carbon nanotube reinforcement of a filament winding resin, in: *47th Internat. SAMPE Sympos*., pp. 1775–1787 (2002).
26. H. Yoshida, T. Ogasa and R. Hayashi, Statistical approach to the relationship between ILSS and void content of CFRP, *Compos. Sci. Technol.* **25**, 3–18 (1986).
27. K. J. Bowles and S. Frimpong, Void effects on the interlaminar shear strength of unidirectional graphite fiber reinforced composites, *J. Compos. Mater.* **26**, 1487–1509 (1992).
28. S. R. Ghiorse, Effect of void content on the mechanical properties of carbon/epoxy laminates, *SAMPE Quarterly*, 54–59 (1993).
29. M. R. Wisnom, T. Reynolds and N. Gwilliam, Reduction in interlaminar shear strength by discrete and distributed voids, *Compos. Sci. Technol.* **56**, 93–101 (1996).
30. N. L. Hancox, The effects of flaws and voids on the shear properties of CFRP, *J. Mater. Sci.* **12**, 884–892 (1977).
31. E. Casal, M. Granda, J. Bermejo, J. Bonhomme and R. Menéndez, Influence of porosity on the apparent interlaminar shear strength of pitch-based unidirectional C–C composites, *Carbon* **39**, 73–82 (2001).